

# Journal of Materials Chemistry B

Accepted Manuscript



This is an *Accepted Manuscript*, which has been through the Royal Society of Chemistry peer review process and has been accepted for publication.

*Accepted Manuscripts* are published online shortly after acceptance, before technical editing, formatting and proof reading. Using this free service, authors can make their results available to the community, in citable form, before we publish the edited article. We will replace this *Accepted Manuscript* with the edited and formatted *Advance Article* as soon as it is available.

You can find more information about *Accepted Manuscripts* in the [Information for Authors](#).

Please note that technical editing may introduce minor changes to the text and/or graphics, which may alter content. The journal's standard [Terms & Conditions](#) and the [Ethical guidelines](#) still apply. In no event shall the Royal Society of Chemistry be held responsible for any errors or omissions in this *Accepted Manuscript* or any consequences arising from the use of any information it contains.

## pH-Responsive Hydrogel Cubes via Sequential Polymer Assembly: Synthesis and Release of Doxorubicin in Cancer Cells

*Veronika Kozlovskaya,<sup>1‡</sup> Jun Chen,<sup>1‡</sup> Chrysanty Tedjo,<sup>1</sup> Xing Liang,<sup>1</sup> Javier Campos-Gomez,<sup>2</sup> Jonghwa Oh,<sup>3</sup> Mohammad Saeed,<sup>2</sup> Claudiu T. Lungu,<sup>3</sup> and Eugenia Kharlamieva<sup>1\*</sup>*

<sup>1</sup>Department of Chemistry, University of Alabama at Birmingham, Birmingham, AL, USA

<sup>2</sup>Department of Biochemistry and Molecular Biology, Southern Research Institute, Drug Discovery Division, Birmingham, AL, USA

<sup>3</sup>Department of Environmental Health Sciences, University of Alabama at Birmingham, Birmingham, AL, USA

\*Correspondence address: 901 14<sup>th</sup> St South, CHEM294, Birmingham, AL, USA, 35294, [ekharlam@uab.edu](mailto:ekharlam@uab.edu)

‡These authors equally contributed to this work

KEYWORDS: Shaped colloids, layer-by-layer, cubic hydrogel particles, pH-responsive networks, triggered release

### ABSTRACT

We report on a novel type of shaped hydrogel microparticles which undergo large, rapid, and reversible volume changes in response to solution pH. The cubic hydrogels are produced as interconnected poly(methacrylic acid) (PMAA) network replicas of mesoporous manganese oxide templates by sequential infiltration of (PMAA) and poly(N-vinylpyrrolidone) (PVPON), followed by cross-linking of PMAA and template dissolution. The integrated advantages of the porous cubic sacrificial templates and responsive PMAA matrix enable synthesis of monodisperse and pH-sensitive hydrogel cubes in a rapid, facile, and reproducible manner. These hydrogel cubes display a reversible 2-fold change in size while maintaining their shape in response to pH variations. The swelling behavior of cubic and spherical hydrogel particles is controlled by the network structure which is regulated by the PMAA molecular weight. These networks maintain their three-dimensional shapes in the dry state. No cytotoxicity is found for cubic and spherical hydrogels upon their interactions with human cancer cells for various time intervals. Finally, pH-triggered loading and release of doxorubicin to and from the cubic hydrogels is shown and their anticancer effect is demonstrated. The viability of A549 and HeLa cancer cells was significantly decreased upon interaction with doxorubicin-loaded cubic hydrogels. The approach presented here provides a new platform of multi-functional particles

with highly-controlled geometry, size, composition, and responsive properties to be potentially used in targeted drug delivery for cancer therapy.

## INTRODUCTION

Stimuli-responsive hydrogels hold considerable potential as materials with reversible property transformations. These three-dimensional networks exhibit the unique ability to drastically and reversibly change volume when either swelling or shrinking.<sup>1,2</sup> Due to their biocompatibility and flexible methods of synthesis, hydrogel structures have numerous applications in drug delivery, tissue engineering, and sensing.<sup>3</sup> Although many types of microgels with finely-tuned chemical and physical properties have been developed over the past several decades, they mostly include spherical structures.<sup>4</sup> However, shape plays an important role in functions of polymer particulates, along with size and surface chemistry.<sup>5,6,7</sup> Particle shape affects cellular uptake, vascular dynamics and circulation,<sup>8-14</sup> all of which are crucial for drug delivery.<sup>8,9,15-17</sup> For instance, worm-shaped polymer particles showed negligible phagocytosis compared to spheres of the same volume.<sup>18</sup> Rod-like<sup>19</sup> and discoidal particles<sup>20</sup> demonstrate increased blood circulation time and exhibit a much higher margination (drifting towards the walls) under flow than the spherical systems, thus reducing their clearance in the liver or spleen.<sup>18,19,21-23</sup> Oblate particles adhere more efficiently to the vascular endothelium than do spheres of the same volume.<sup>10</sup>

There are only a few examples of responsive non-spherical hydrogels. For instance, rod-like protein-based microgels have been produced which bend reversibly in response to the chemical environment.<sup>24</sup> Reconfigurable hydrogel/PLGA multicompartamental microcylinders underwent reversible bending and toggling due to interfacial stresses under exposure to ultrasound or an appropriate solvent.<sup>25</sup> The paucity of hydrogel-based shape-defined structures is likely due to their poor mechanical stability.<sup>26</sup> In contrast, the highly cross-linked micro-sized networks obtained by microfluidics, lithography, and PRINT, offer excellent control over shape and size but they lack capabilities of dynamic volume changes.<sup>27</sup> Apparently, stimuli-triggered volume transitions require the spatial conditions for polymer chain rearrangement that is not available in particles from those processes.

Layer-by-layer (LbL) technology offers unique opportunities to synthetically recreate shapes and easily impart a desired elasticity and responsiveness to multilayer material.<sup>28,30,31</sup> Stimuli-

responsive multilayer capsules are formed by sequential assembly of weak polyelectrolytes on sacrificial templates followed by template dissolution.<sup>32,33,34</sup> These capsules replicate the geometry of the templates and comprise ultrathin multilayer shells (<50 nm) with sub- or micron size cavities.<sup>35-40</sup> When deposition of multilayers occurs inside porous sacrificial templates, nanoporous particles of interconnected macromolecular networks are formed.<sup>41-43</sup> Porous silica and calcium carbonate particles are the mostly widely used inorganic templates, due to their size monodispersity, ease of preparation, large surface area, and controllable pore size during synthesis.<sup>44-46</sup> For instance, nanoporous spheres of cross-linked poly(acrylic acid) (PAA) and poly(allylamine hydrochloride) (PAH) were obtained via stepwise infiltration of these macromolecules into the mesoporous silica particles.<sup>47</sup> Porous CaCO<sub>3</sub> microparticles with an average pore size of 35 nm were utilized for synthesis of poly(styrene sulfonate)(PSS)/PAH microcapsules with an internal polyelectrolyte matrix.<sup>41,48</sup> The resulting porous polymer particles were shown to be used for loading and release of proteins triggered by changes in solution pH.<sup>41,43</sup> Recently, nanoporous particles of thiolated poly(methacrylic acid) were prepared by mesoporous silica templating and showed rapid internalization by HeLa cells.<sup>49</sup>

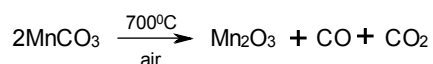
Unlike other template methods of particle synthesis,<sup>50</sup> the LbL-assisted approach is facile, versatile, and allows for deposition in aqueous environment, all relevant to biological applications. One of LbL-assembly's key advantages over the traditional bulk polymerization techniques is the nanoscale control over composition, structure, and morphology of porous polymer particles which is inherent to the technique.<sup>51</sup> However, the traditional bulk-polymerized nanoporous particles hold several benefits over LbL capsules. These porous polymer particles can maintain their shape and structural integrity in the dry state, unlike polyelectrolyte capsules which totally collapse upon drying.<sup>43</sup> In addition, their interconnected nanoporous matrix-type structure allows for improved loading efficiency due to both adsorption and physical entrapment mechanisms of cargo incorporation.<sup>41,43</sup> In contrast, encapsulation is mostly through molecular entrapment inside the capsule interior due to the limited surface area of capsule wall allowed for adsorption. Despite these unique properties, the LbL-template synthesis of hydrogel particles has been rarely explored and limited to spherical structures.<sup>49</sup> The lack of studies on microgels of non-spherical shapes can be explained by limitations in particle design, mostly limiting studies to spherical templates.

Herein, we report on synthesis of a novel type of stimuli-responsive nanoporous hydrogel microparticles of cubic shape and their interactions with human cancer cells. We illustrate that these cubic hydrogels maintain their three-dimensional shapes in the dry state and undergo large, rapid, and reversible volume changes in response to solution pH. Recently, we demonstrated pH-responsive poly(methacrylic acid) (PMAA)-based capsules of cubic shape prepared as hollow replicas of manganese carbonate templates through chemical cross-linking of hydrogen-bonded multilayers.<sup>52,53</sup> In the current work, the cubic PMAA hydrogels are formed by sequential infiltration of PMAA and poly(N-vinylpyrrolidone) (PVPON) into the cubic mesoporous manganese oxide templates, followed by chemical cross-linking of PMAA and template dissolution. The effects of PMAA molecular weight, template porosity, and hydrogel size on the structural integrity and pH-responsive swelling of cubic microgels are investigated. The swelling behavior of the hydrogel cubes is compared to that of hydrogel spheroids and cubical hydrogel capsules. Cytotoxic properties of these networks are studied upon their interaction with human cancer cells for various time intervals. Finally, pH-triggered loading and release of doxorubicin to and from cubic hydrogels, and their anticancer effect are explored on A549 and HeLa cancer cells. The presented approach is simple, robust and integrates the advantages of shape and pH-sensitivity to develop novel types of shape-specific ‘intelligent’ networks with programmable behavior to be used for storage and delivery of functional cargo.

## RESULTS AND DISCUSSION

### **Fabrication of porous templates from cubic and spherical manganese carbonate particles**

Porous manganese oxide particles of cubic and spherical geometries were synthesized and used as sacrificial templates for the correspondingly shaped hydrogels. To obtain porous templates, monodisperse cubic and spherical  $\text{MnCO}_3$  microparticles were produced as developed previously<sup>52</sup> and heated at  $700^\circ\text{C}$  for 3 hours (Figure 1a-b).<sup>54</sup> Manganese carbonate particles have been selected due to their controllable size and shape during synthesis.<sup>52</sup> Figure 2 demonstrates that initially smooth and cubic  $\text{MnCO}_3$  particles of  $2.1\pm 0.1\ \mu\text{m}$  in size showed highly porous surface morphology after 3 hours of calcination. The transformation of  $\text{MnCO}_3$  to manganese oxide (III) follows the chemical reaction:<sup>54</sup>



SEM images of the broken  $\text{Mn}_2\text{O}_3$  particle clearly displays the porous structure inside (inset in Fig. 2d). Similarly,  $\text{MnCO}_3$  spheres of  $2.4 \pm 0.1 \mu\text{m}$  transformed into porous  $\text{Mn}_2\text{O}_3$  particles after heat treatment (Fig. 2a-d). Despite these particles having rough surfaces, their porous morphology is clearly observed with SEM (Fig. 2d). No changes in particle shape or size were observed after the heat treatment. Table 1 summarizes the properties of porous manganese oxide particles obtained by the BET method. The analysis revealed similar surface areas of  $17.5 \text{ m}^2 \text{ g}^{-1}$  for two types of cubic particles. The pore sizes varied from 14 to 89 nm with the average pore size of 44 nm for the 2- $\mu\text{m}$  cubes and from 3 to 80 nm with the average pore size of 40 nm for the 4- $\mu\text{m}$  cubes. These average pore sizes are larger than those in porous spherical particles of  $\text{CaCO}_3$  (35 nm) and mesoporous silica (a bimodal pore structure of 3 nm and 10-40 nm) previously used for template synthesis of porous polymer particles.<sup>32,41,43,49</sup> In our case, the surface area of porous  $\text{Mn}_2\text{O}_3$  is two-fold greater than that reported for porous  $\text{CaCO}_3$  microparticles.<sup>41</sup>

**Table 1.** Properties of Cubic and Spherical Porous Manganese Oxide Templates.

Particles	Average Pore Size <sup>a</sup> (nm)	Surface Area <sup>b</sup> ( $\text{m}^2 \text{ g}^{-1}$ )	Pore Volume <sup>c</sup> ( $\text{cm}^3 \text{ g}^{-1}$ )
2 $\mu\text{m}$ cubic	44	$17.5 \pm 0.4$	$0.192 \pm 0.002$
4 $\mu\text{m}$ cubic	40	$17.5 \pm 0.5$	$0.175 \pm 0.004$
2 $\mu\text{m}$ spherical	43	$19.3 \pm 0.5$	$0.205 \pm 0.005$

<sup>a,b</sup> Calculated from the BET method, <sup>c</sup> Calculated by the Barrett-Joyner-Halender (BJH) method from the desorption curve.

We also found the average surface area ( $19.3 \text{ m}^2 \text{ g}^{-1}$ ) and porosity of 2- $\mu\text{m}$  spheres to be similar to those obtained for the cubes. The spherical particles demonstrated the average pore size of 43 nm with the pore size variations from 15 to 80 nm (Table 1). Although the BET analysis showed no significant difference in overall pore sizes and volumes, SEM revealed variation in pore sizes on particle surfaces. The surface pore dimensions fall in the range from 40 to 80 nm for 2- $\mu\text{m}$  cubic templates, while 20-40 nm pores were observed for both 2- $\mu\text{m}$  spherical and 4- $\mu\text{m}$  cubes

(Fig. 2, Fig. S1). This discrepancy in pore sizes is important to consider for polymer infiltration within the particles, which will be discussed later in the manuscript.

Surface charge measurements of the initial manganese carbonate and final manganese (III) oxide cores revealed that after calcination the templates acquired a highly negative surface charge in solutions at pH=3.6. The  $\zeta$ -potential value decreased from  $7\pm 3$  to  $-45\pm 3$  mV for 2- $\mu\text{m}$   $\text{MnCO}_3$  and  $\text{Mn}_2\text{O}_3$ , respectively (Fig. 3a). We also found that 4- $\mu\text{m}$  cubic porous templates exhibited similar  $\zeta$ -potential of  $-45.5\pm 0.2$  mV at pH=3.6, indicating no effect of particle size on its  $\zeta$ -potential (Fig. 3a). Likewise, no effect of particle shape on particle  $\zeta$ -potential was found after the heat-induced particle transformation. Thus, highly negative  $\zeta$ -potential values of  $-41.3\pm 0.4$  mV and  $-45\pm 3$  mV were observed for porous 2- $\mu\text{m}$  spheres and cubes, respectively (Fig. 3b). Importantly, this highly negative surface charge of the porous templates favors the particle stability against aggregation in solution.

### Fabrication of hydrogel particles of cubic shape

Cubic PMAA hydrogels were produced by the selective cross-linking of PMAA in hydrogen-bonded (PMAA/PVPON) multilayers, followed by template dissolution (Fig. 1). The multilayers of PMAA and PVPON were deposited stepwise inside the 2- $\mu\text{m}$  porous cubic templates by exposing them to the polymer solutions at pH=3.6 (Fig. 1b-c). PMAA of two different molecular weights such as  $21,800 \text{ g mol}^{-1}$  and  $350,900 \text{ g mol}^{-1}$  denoted as 21 kDa or 'short' and 360 kDa or 'long' PMAA, respectively, were used. To promote the multilayer assembly, aqueous PEI solution was deposited before the multilayer assembly. After the sequential infiltration of seven (PMAA/PVPON) bilayers, the on-template assembly was cross-linked with ethylenediamine using carbodiimide-assisted method followed by exposure to pH=8.5, as developed previously for PMAA capsules.<sup>34,55</sup> This procedure resulted in PVPON release due to disruption of hydrogen bonds between PVPON and deprotonated PMAA leading to one-component PMAA networks inside the pores (Fig. 1d). The infiltration procedure was followed by  $\zeta$ -potential measurements before and after hydrogel formation on templates. Figure 3c demonstrates that the  $\text{Mn}_2\text{O}_3$  templates has a highly negative surface charge, showing  $\zeta$ -potentials of  $-42\pm 2$  mV and  $-59\pm 2$  mV at pH=3.6 and 7.0, respectively. The presence of the (PMAA)<sub>7</sub> network inside the template drastically reversed the  $\zeta$ -potential to positive values of  $24.8\pm 0.1$  mV and  $25\pm 2$  mV for short and long PMAA, respectively, at pH=3.6. These particles

reversed to the negative  $\zeta$ -potentials of  $-34\pm 2$  mV and  $-33\pm 2$  mV, for short and long PMAA, respectively, at pH=7.0. The pH-triggered variations in the  $\zeta$ -potential value of the hydrogel-modified templates are due to the amphoteric nature of the PMAA networks cross-linked with ethylenediamine.<sup>56,57</sup> The excess positive charge at acidic pH is induced by the presence of one-end-attached protonated ethylenediamine groups remaining after cross-linking. The excess negative charge at neutral pH is due to ionized uncross-linked carboxylic groups in the PMAA network (Fig. 3c).

To obtain PMAA hydrogels, 2- $\mu$ m inorganic templates with cross-linked PMAA of both 21 kDa and 360 kDa were exposed to 1 M hydrochloric acid (Fig. 1d). This procedure resulted in  $\text{Mn}_2\text{O}_3$  dissolution and the formation of cubically shaped hydrogels. As demonstrated by the three-dimensional (3D) CLSM images, the (PMAA)<sub>7</sub> networks of both short and long PMAA preserved the cubic shapes of the templates after the template dissolution (Fig. 4a,b). The residues of manganese ions remaining after the template dissolution were removed by treatment with 0.1 M EDTA at pH=7 for 3 hours, followed by dialysis in deionized water. Energy dispersive X-ray spectroscopy revealed no signal from manganese (0.637 keV) and proved the absence of the manganese ions inside 2- $\mu$ m PMAA hydrogel cubes (Inset, Fig. 4a). For CLSM visualization, the hydrogel particles were allowed to interact with Alexa-488 fluorescent dye. The corresponding orthogonal (side) views of 3D confocal images in Figures 4c and 4d demonstrate that the hydrogel cubes are homogeneously filled with the fluorescent dye, a feature observed earlier in spherical gel-like particles.<sup>41</sup> These results indicate that despite the shape anisotropy, the interconnected network is uniformly distributed throughout the volume of 2- $\mu$ m cubic hydrogels.

Remarkably, we have found that the obtained 2- $\mu$ m (PMAA)<sub>7</sub> hydrogels maintain their cubic self-supported shape in dry state. The SEM images clearly show that both short- and long-(PMAA)<sub>7</sub> hydrogels preserve their structural integrity upon drying as evidenced by their well-defined corners and faces (Fig. 5a,d).

To explore the effect of size and shape on hydrogel integrity, 4- $\mu$ m cubic and 2- $\mu$ m spherical porous templates were used for (PMAA)<sub>7</sub> network fabrication. We found that PMAA molecular weight plays a significant role in the structure and integrity of 4- $\mu$ m cubic and 2- $\mu$ m spherical hydrogels. In contrast, no effect of PMAA molecular weight was found for 2- $\mu$ m cubes as

discussed above. The SEM images of dry 4- $\mu\text{m}$  cubic and 2- $\mu\text{m}$  spherical hydrogels made of short PMAA (21 kDa) clearly display self-supported structures (Fig. 5b,c). In drastic contrast, these systems lost the three-dimensional structure after drying if made of long PMAA (360 kDa). As seen from SEM, both 4- $\mu\text{m}$  cubic and 2- $\mu\text{m}$  spherical systems collapsed in dry state (Fig. 6e,f). However, the surface morphology of these dry spheres and cubes is relatively smooth, indicating thicker walls when compared to previously shown highly-wrinkled structures of ultrathin PMAA capsules made on solid templates.<sup>52</sup> Note that when 20-layer PMAA cubic capsules were formed on non-porous 4- $\mu\text{m}$   $\text{MnCO}_3$  particles, the template-free PMAA capsules totally collapsed upon drying, due to the much thinner hydrogel wall ( $\sim 30$  nm in thickness<sup>52</sup>) (Inset in Fig. 5f).

These results can be rationalized based on the average pore sizes of the porous manganese (III) oxide particles. We found that exposure of all types of  $\text{MnCO}_3$  particles for 3 hours at  $700^\circ\text{C}$  resulted in the nanoporous templates with similar average pore sizes (around 40 nm) as measured by the BET method (Table 1). However, the SEM analyses revealed variations in pore size on particle surfaces. Thus, the 2- $\mu\text{m}$  porous manganese oxide cubes showed 40-80 nm pores, while both 2- $\mu\text{m}$  spheres and 4- $\mu\text{m}$  cubes had 20-40 nm pores (Fig. 2 and S1). The estimated radii of gyration for PMAA ( $M_w=21,800$  g mol<sup>-1</sup>) and PVPON ( $M_w=13,200$  g mol<sup>-1</sup>) in solution at low deposition pH=3.6 are 1.8 nm and 2.2 nm, respectively, assuming corresponding persistence lengths of 0.3 nm and 1 nm.<sup>58,59,60</sup> Since the diameters of the PMAA and PVPON coils (3.6 nm and 4.4 nm, respectively) are much smaller than the pore diameters, the molecules could easily infiltrate inside the 2- $\mu\text{m}$  cubic templates with 40-80 nm pores. Similarly, the  $R_g$  for PMAA with  $M_w=350,900$  g mol<sup>-1</sup> is estimated to be 7.24 nm (the diameter of  $\sim 14.5$  nm) which permits the assembly inside these templates. In contrast, when the surface pore size is 20-40 nm, the effect of PMAA molecular weight on the hydrogel particle formation becomes more pronounced. The 4-fold increase in the PMAA diameter from 3.6 nm to 14.5 nm leads to the limited diffusion because the size of PMAA 360 kDa is comparable to the 20-40 nm pores. In this case, the formation of capsule-like structures with thick walls instead of filled hydrogel particles is observed due to a fast pore “clogging” (Fig. 5e,f). These results correlate well with the previously shown decreased infiltration of poly(acrylic acid) corresponding with the decrease in pore size of nanoporous silica spheres.<sup>61</sup> The limited diffusion of PSS/PAH into porous  $\text{CaCO}_3$

and porous silica was also found to result in capsule-like structures with thick walls due to formation of polyelectrolyte complexes on the surface of those particles.<sup>41</sup>

### Responsive properties of shaped hydrogel particles

Responsive behavior of cubic and spherical hydrogel particles was explored using confocal microscopy. First, cubic hydrogels made on 2- $\mu\text{m}$  cubic templates were investigated. We found that the cubic PMAA hydrogels showed pH-dependent swelling ratios of 1.7, defined as the ratio of swollen to deswollen hydrogel particle size. Hydrogel cubes made from 21 kDa PMAA increased in size from  $1.9\pm 0.2\ \mu\text{m}$  to  $3.2\pm 0.1\ \mu\text{m}$  when the solution pH was changed from pH=5 to pH=7.4 (Fig. 6a, b, c). Similarly, cubic hydrogels of 360 kDa PMAA changed from  $1.9\pm 0.2\ \mu\text{m}$  to  $3.1\pm 0.2\ \mu\text{m}$ , resembling the previous pH variations and indicating no effect of PMAA molecular weight on cubic hydrogel pH-responsive behavior. The similar swelling behavior of these systems can be attributed to their comparable structures showing uniform networks inside the particles as confirmed with SEM (Fig. 5a, b). The pH-triggered volume changes were completely reversible (Fig. 6c).

Remarkably, these hydrogels retained their cubic geometry upon pH changes, indicating uniform swelling/shrinkage of the networks. It was previously shown that spherical capsules of cross-linked PMAA underwent  $\sim 2$ -fold increase in size when exposed from slightly acidic to basic pH.<sup>56,57</sup> This behavior is dictated by the pH-responsiveness of the hydrogel capsule wall which shrinks at slightly acidic pH but swells at basic pH due to self-repulsion between ionized carboxylic groups. We also found previously that cubic (PMAA)<sub>20</sub> capsules transformed in shape to become spherical upon pH increase from pH=5 to pH=7.4 following EDTA treatment of the capsule wall.<sup>52,53</sup> In contrast to cubic (PMAA)<sub>20</sub> capsules, cubic (PMAA)<sub>7</sub> hydrogel particles presented here preserve their cubic geometry in the swollen state at pH=7.4. This difference in shape responses can be attributed to the improved robustness and rigidity of the interconnected network unlike the easily-deformable and soft ultrathin capsule wall. Indeed, the more rigid two-component (PMAA-PVPON)<sub>5</sub> capsules retained their cubic shape while increasing in size upon pH-induced variations.<sup>53</sup> However, the swelling ratio of the cubic (PMAA-PVPON) capsules was lower than that for cubic (PMAA) hydrogels studied here (1.3 versus 1.7, for the previous capsules and current hydrogels, respectively).

Next, cubic hydrogel particles prepared on 4- $\mu\text{m}$  cubic templates were explored. We found that the cubic hydrogels (obtained with short PMAA) exhibited a similar 1.7-fold swelling ratio increasing in size from  $2.7\pm 0.2\ \mu\text{m}$  to  $4.7\pm 0.4\ \mu\text{m}$  at pH variations from 5 to 7.4. (Fig. 6d, e, f). Interestingly, 4- $\mu\text{m}$  capsule-like cubic structures (obtained with long PMAA) swelled less than the corresponding 4- $\mu\text{m}$  hydrogel cubes showing swelling ratio of 1.5 and 1.7 for capsules and gels, respectively.

Finally, spherical hydrogels produced using 2- $\mu\text{m}$  spherical porous cores were studied (Fig. 6g, h, i). We found that the swelling behavior of the 2- $\mu\text{m}$  spheres was very similar to that of 4- $\mu\text{m}$  cubic structures. The uniformly filled hydrogel spheres (obtained with short PMAA) had a swelling ratio of  $\sim 1.7$  ( $2.3\pm 0.2\ \mu\text{m}$  at pH=5 and  $4.1\pm 0.2\ \mu\text{m}$  at pH=7.4, respectively) (Fig. 6i). The same result was obtained for the hydrogel cubes of comparable pore dimensions (Fig. 6c). Likewise, spherical capsule-like particles obtained with long PMAA swelled 10% less than the filled hydrogel spheres.

Our overall results indicate that the hydrogel particles, both cubes and spheres, undergo a nearly 2-fold reversible swelling/shrinkage response to pH variations. The hydrogel cubes retained their cubic shape while increasing in size, providing a remarkable example of a pH-responsive shaped hydrogel. The swelling behavior of cubic and spherical hydrogel particles is controlled by the network structure, which is regulated by the PMAA molecular weight and the template properties. Indeed, swelling ratios for the capsule-like hydrogels with thick walls - both spherical and cubic - were typically  $\sim 10\%$  smaller than those for the filled hydrogel particles. The result can be attributed to a smaller amount of material assembled into the capsule-like particles compared to that of the filled hydrogel particles. Another interesting observation is that uniformly filled hydrogel cubes and spheres exhibit similar swelling ratio of 1.7-fold; which suggests similar cross-link densities despite various PMAA molecular weight and hydrogel shape. From our previous study, PMAA hydrogels films and capsules showed 11 monomer units between two cross-links under the same cross-linking conditions.<sup>62</sup>

### **pH-Responsive release of doxorubicin (DOX) from cubic hydrogels**

We explored pH-induced loading and release of DOX, a drug used for treatment of a wide range of cancers, in the PMAA hydrogel particles as a result of pH-regulated ionic interactions

between DOX and the PMAA hydrogel. Figure 7 shows that the PMAA hydrogels, regardless of shape or size, possess a negative surface charge with the  $\zeta$ -potential value for the systems oscillating around -30 mV at pH=7.4. The negative charge is attributed to ionization of the carboxylic groups in the swollen PMAA matrix (Fig. 6c, f, i). The  $\zeta$ -potential drops to slightly negative values (in the range from 0 mV to -10 mV) at pH=5 due to protonation of PMAA (Fig. 7). These pH-dependent charge variations of PMAA matrix were exploited for DOX loading and release. Cubic hydrogel particles were soaked in DOX solution at pH=6.4 for 24 h followed by rinsing at pH=7.4 to induce electrostatic interactions of positively charged DOX ( $pK_a=8.3$ ) and the ionized PMAA hydrogel. Confocal microscopy was used to visualize DOX distribution inside the particles. We found that the loading efficiency can be controlled by the structure of the hydrogel particles. As observed with confocal microscopy, the cubic and spherical hydrogels were uniformly filled with the drug throughout the particle volume as evidenced by the uniform fluorescence from DOX (Fig. 8a, c, e). In contrast, capsule-like thick-walled cubes and spheres displayed fluorescent frames with unfilled dark cavities indicating drug accumulation at the capsule walls (Fig. 8d, f). These results on visualized particle structures correlate well with the morphology of the dry hydrogel systems observed with SEM (Fig. 5). Cubic and spherical hydrogels with a uniform network structure (Fig. 8a, b, c, e) maintained their 3D structural integrity by preserving their shape upon drying (Fig. 5a, b, c, d). In contrast, capsule-like hydrogel particles with thick walls, which were clearly observed with confocal microscopy (Fig. 8d, f), collapsed in the dry state (Fig. 5e, f). Upon DOX loading, the size of the hydrogel cubes decreased due to the electrostatic interactions between DOX and PMAA network. For instance, the size of the 4- $\mu$ m hydrogel cubes decreased from  $4.7\pm 0.2$  to  $2.7\pm 0.2$   $\mu$ m before and after drug loading, respectively, (Fig. 9a, b). A similar contraction was observed previously with spherical PMAA capsules exposed to polycationic quaternized poly(4-vinylpyridine).<sup>55</sup> Importantly, the shape of the DOX-loaded hydrogel particle remained cubic at pH=7.4, which can be important for shape-regulated delivery of active molecules (Fig. 9a, b).

To investigate the release of DOX, drug-loaded cubic hydrogels were exposed stepwise to a series of solutions with pH ranging from 7.4 to 3 and imaged with confocal microscopy (Fig. 9a-f). Both fluorescence and transmitted light images show that DOX started releasing at pH=5 until its complete disappearance from the cubes at pH=3 (Figs. 9c-f). As seen from the transmitted light images of the hydrogel cubes, the particle size increased at pH=3 reflecting the hydrogel

swelling due to the positive charge of PMAA network at low pH (Fig. 9d, f and Fig. 3c). As a result of DOX release, the network size increased due to the breakage of electrostatic interactions between PMAA hydrogel and DOX. The pH-triggered DOX release from cubic hydrogels was quantified using UV-Vis spectroscopy. DOX was loaded into 2- $\mu\text{m}$  cubic gels of (PMAA)<sub>7</sub> (21 kDa) by incubation of the gel particles in a certain volume of 0.2 mg mL<sup>-1</sup> DOX solution (pH=6.4, 0.01 M phosphate) for 24 h (Fig. 9g). The particle concentration was measured using a hemocytometer (Fisher Scientific). DOX-loaded cubic hydrogel particles were exposed to certain volumes of 0.01 M phosphate buffers at pH=7.4, pH=5, and pH=3 for varied periods of time and the amount of DOX released was obtained from the measurements using the DOX calibration curve ( $\lambda_{\text{max}}=480$  nm). The mass of DOX loaded in the 2- $\mu\text{m}$  cubic hydrogel particles was found to be 0.203 ng particle<sup>-1</sup>. Figure 9h demonstrates that after 24-h exposure of DOX-loaded cubes to pH=7.4 and pH=5, the release was only 4.4 $\pm$ 0.1% and 7.2 $\pm$ 0.1%, respectively. Remarkably, 80 $\pm$ 1% of the loaded DOX was released from the cubes within 1 hour of their exposure to pH=3. These results demonstrate that DOX can be released from PMAA cubic hydrogel particles in the acidic endosomal/lysosomal environment following the particle's being uptaken by a cell.

### **In-vitro cell studies**

Cytotoxicity of polymer matrices is a critical factor for a drug delivery vehicle intended for therapeutic delivery applications. Rigid particles may suffer from tissue toxicity and rapid blood clearance.<sup>18</sup> In this regard, soft porous hydrogel particles are advantageous in contrast to, for instance, micelles or liposomes, because of the mechanical integrity and higher drug loading capacity due to a larger number of functional groups available for interaction with free drug molecules. Moreover, shielding loaded drug molecules from immunologic attack and the capability for further functionalization<sup>63</sup> of a PMAA hydrogel particle for immunomodulatory and targeting purposes makes the hydrogel particles a potentially superior drug carrier.

Although non-cytotoxic properties of the hydrogel matrices of poly(methacrylic acid) cross-linked with disulfide bonds have been reported recently,<sup>64</sup> the presence in the presently-synthesized hydrogel of free primary amine groups left from the reaction of the ethylenediamine cross-linker may, in principle, lead to cell membrane damage and subsequently cytotoxicity.<sup>65</sup> Therefore, the PMAA hydrogel particles were examined to determine if they exhibited any cytotoxicity. Two different human cancer cell lines (HeLa and HEK293) were used in the

experiments. The hydrogel particles, 2- and 4- $\mu\text{m}$  cubes made of 21 kDa PMAA, and 2- $\mu\text{m}$  cubes and spheres made of 21 and 360 kDa PMAA, respectively, were incubated with the cells at the particle-to-cell ratio of 100:1. At 24-h intervals (Days 1, 2, and 3), cell viability was determined in each cell culture by CellTiter-Glo luminescent cell viability assay. This method allows determining the number of viable cells in a culture based on quantitation of intracellular adenosine triphosphate, which signals the presence of metabolically-active (live) cells. The viability data for each type of the hydrogel particles were obtained as an average of six replicates for each group. Figure 10a shows the representative optical image of a an optical plane within A549 (human alveolar adenocarcinoma) cells with the internalized cubic hydrogel particles (2- $\mu\text{m}$  cubes made of 21 kDa PMAA) with cell nuclei stained blue (DAPI) and actin filaments stained red with Alexa Fluor-594-conjugated phalloidin. Figures 10b-c demonstrate that the cell viability in cultures incubated with each particle type was not significantly different than in the untreated group. Together, these data clearly indicate that PMAA hydrogel particles, regardless of shape (spherical or cubic), or size (small, 2- $\mu\text{m}$  or large, 4- $\mu\text{m}$ ) do not exert any significant cytotoxicity to the studied cells and can be further explored for drug delivery.

To explore the drug delivery capability of hydrogel cubes, the 2- $\mu\text{m}$  cubes were loaded with DOX, and incubated with A549 and HeLa cancer cells at cell-to-particle ratio of 1:100. Particle-free supernatant of the DOX-cubes suspension was used as a negative control with the same volume as that of DOX-cubes suspension. DOX solution (1 $\mu\text{M}$ ) was used as a positive control of cytotoxicity. Subsequently, the percent of viable cells compared to the negative control was measured after 24-, 48-, and 72-h incubation. The data in Figure 11 show that the incubation of the A549 cells with DOX-cubes resulted in a gradual cell cytotoxicity from 25% to 40% after 24 h and 72 h of incubation, respectively, which was comparable to that observed for free DOX used at the reported  $\text{IC}_{50}$  concentration (1 $\mu\text{M}$ )<sup>66</sup> (Fig. 11a). For HeLa cells, the cytotoxicity from the DOX-cubes was observed already in 24 h and was similar to that observed for A549 cells causing ~40% cell death in 72 h. These results indicate that a drug loaded in the hydrogel cubes can be effectively delivered to the interior of cells. The data demonstrate potential of the hydrogel cubes loaded with DOX for pH-responsive delivery of the anticancer drug in cancer cells.

## CONCLUSIONS

We presented the first example of pH-responsive cubic PMAA hydrogels made with an LbL template synthesis method on mesoporous manganese oxide templates of cubic geometry. Hydrogel particles, both cubes and spheres, underwent reversible 2-fold swelling/shrinkage in response to pH variations. The hydrogel cubes retained their cubic shape while changing in size. We found the structural integrity and pH-responsive swelling properties of cubic and spherical hydrogels to be significantly affected by PMAA molecular weight and template porosity. Cubic and spherical hydrogels with a uniform network structure maintained their 3D structural integrity by preserving their shapes upon drying. In contrast, capsule-like hydrogel particles with thick walls, clearly observed with confocal microscopy, collapse upon drying. Swelling ratios for the capsule-like hydrogels with thick walls, both spherical and cubic, were typically ~10% smaller than those for the filled hydrogel particles. No cytotoxicity was found for these networks as investigated upon their interaction with human cancer cells for various time intervals. We also showed pH-triggered loading and release of doxorubicin to and from cubic gels. Finally, when A549 and HeLa cancer cells were incubated with 2- $\mu\text{m}$  DOX-loaded cubic hydrogels, cell viability was significantly decreased. The presented approach is simple, robust and integrates advantages of shape and pH-sensitivity to develop novel types of shape-specific ‘intelligent’ networks with programmable behavior to be used for storage and delivery of functional cargo.

ACKNOWLEDGEMENT. This work was supported by NSF-DMR1306110 (EK) and funds from Southern Research Institute (MS). Mr. W. Higgins (UAB) is acknowledged for technical assistance.

## EXPERIMENTAL

**Materials.** Poly(ethyleneimine) (PEI, average  $M_w$  25,000), ethylenediamine (EDA), manganese sulfate monohydrate and ammonium bicarbonate were purchased from Sigma-Aldrich. 1-Ethyl-3-(3-(dimethylamino)propyl)-carbodiimide hydrochloride (EDC) was obtained from Chem-Impex International. Poly(methacrylic acid) (PMAA, average  $M_w$  21,800 g mol<sup>-1</sup>, PDI=1.32 ; and 350,900 g mol<sup>-1</sup>, PDI= 2.05) were from Sigma-Aldrich and Polysciences Inc, respectively. Ultrapure de-ionized water with a resistivity of 0.055  $\mu\text{S}/\text{cm}$  was used in all experiments (Siemens). Monobasic and dibasic sodium phosphate (Fisher Scientific) were used for preparation of polymer solutions if otherwise was not mentioned. Doxorubicin hydrochloride was purchased from LC Laboratories (USA). Poly(N-vinylpyrrolidone) (PVPON,  $M_w$  13,200 g

$\text{mol}^{-1}$ , PDI=1.20) was synthesized using modified RAFT polymerization described elsewhere.<sup>67</sup> Briefly, N-vinylpyrrolidone (3.3 g; 30 mmol), Rhodixan A1 (31 mg; 0.15 mmol), AIBN (13 mg; 0.08 mmol) and 1,4-dioxane (2 g) were placed in a Schlenk flask equipped with a magnetic stirrer. The solution was degassed by three freeze-pump-thaw cycles and set under argon atmosphere and heated at 60°C for 12 h. The polymerization was stopped by quenching in liquid nitrogen. The obtained PVPON was precipitated in hexane and filtered. The polymer was purified by dialysis in deionized water for 3 days using a Float-A-lyzer device with 8 kDa cutoff (SpectrumLabs).

**Synthesis of porous cubic and spherical microparticles.** Cubic and spherical manganese carbonate cores of various sizes were synthesized as described previously.<sup>52,39</sup> Briefly, fresh nano-seed solution was prepared by mixing 0.04 g  $\text{NH}_4\text{HCO}_3$  and 0.02 g  $\text{MnSO}_4$  in 200 mL DI water. Then, 100 ml of the nano-seed solution was added to 500 mL of 6 mM  $\text{MnSO}_4$  containing 0.5% 2-propanol. Then 500 mL of 0.06 M ammonium bicarbonate solution with 0.5% of 2-propanol were poured into the nano-seed solution. The mixture was immediately heated at 80°C for 30 minutes to result in 2  $\mu\text{m}$  cubic manganese carbonate particles. For 4  $\mu\text{m}$  cubic particles, 70 mL of the nano-seed solution was added to the  $\text{MnSO}_4$  solution. For  $\text{MnCO}_3$  spherical cores, 300 mL of 0.06 M  $\text{MnSO}_4$  solution were heated to 60°C, and 100 mL of the nano-seed solution and 300 mL of 0.06 M ammonium bicarbonate solution were poured into the  $\text{MnSO}_4$  solution. The mixture was stirred vigorously for 15 minutes at 80°C. All the  $\text{MnCO}_3$  particles (cubes and spheres) were collected by filtering through 0.45  $\mu\text{m}$  Whatman filters, rinsed with DI water several times and dried at room temperature ( $\sim 25^\circ\text{C}$ ). Obtained solid carbonate particles were heated at 700° C for 3 h to result in porous particles of a similar shape.

**Fabrication of nanoporous hydrogel particles.** Nanoporous hydrogel particles of various shapes were made by depositing seven hydrogen-bonded bilayers of PMAA/PVPON inside pores of the porous particles. Typically, porous templates were exposed to 1.5  $\text{mg mL}^{-1}$  of polymeric solution at pH=3.6 for 45 min (15 min sonication and 30 min shaking). After each deposition step the particles were centrifuged at 6000 rpm for 5 min, and re-suspended in a 0.01 M phosphate at pH=3.5. The rinsing was performed two times before the next deposition step. Before deposition of (PMAA/PVPON) layers, porous particles were exposed to aqueous PEI solution (1.5  $\text{mg mL}^{-1}$ , 1 h) to enhance the following multilayer adsorption to the pore surfaces.

The PMAA layers were then cross-linked with ethylenediamine. For this, the carboxylic groups on the PMAA layers were first activated with carbodiimide solution (5 mg mL<sup>-1</sup>, pH=5 (0.01 M phosphate) for 30 min, followed by four rinses with 0.01 M phosphate at pH=4.6 and then cross-linked with ethylenediamine (12 μL mL<sup>-1</sup> in 0.01 M phosphate at pH=5) for 16 h followed by four rinses with 0.01 M phosphate at pH=4.6. PVPON was released from the core-shells by their exposure to pH=9. Nanoporous shaped hydrogel particles were obtained after dissolving the template in 1 M HCl solution for 6 h followed by six rinsing steps with acidic water (pH=2). After that, hydrogel particles were exposed to ethylenediamine tetraacetic acid disodium salt (EDTA, 0.1 M) solution at pH=7 for three hours followed by dialysis in deionized water for 3 days. DOX was loaded into hydrogel particles or thick-wall capsules by exposing settled particles to 10 mg mL<sup>-1</sup> DOX solution in 0.01 M phosphate buffer at pH=6.4 overnight. After that, supernatants were removed and particles were rinsed 5 times with 0.01 M phosphate solutions at pH=7.4 and imaged in a Lab-Tek chambered coverglass (Electron Microscopy Sciences). For pH-induced release of DOX, solutions in the chambers with DOX-loaded hydrogel particles were exchanged stepwise for 0.01 M phosphate solutions with pH=5, pH=3, and pH=7.4.

**Confocal laser scanning microscopy (CLSM).** pH-response of the nanoporous hydrogel particles was studied using Zeiss LSM 710 confocal microscope equipped with a 63x oil immersion objective. A drop of a hydrogel particle suspension was added to a chambered coverglass filled with buffer solutions at a certain pH value and images were taken after the particles settled at the bottom of the chamber. For CLSM visualization, the particles were soaked in Alexa-488 fluorescent dye aqueous solution overnight, rinsed 3 times with 0.01 M phosphate solutions at pH=7.4 and analyzed with CLSM.

**Scanning electron microscopy (SEM).** SEM analysis was performed using a FEI Quanta<sup>TM</sup> FEG microscope at 10 kV. Samples were prepared by depositing a drop of a particle suspension on a silicon wafer or carbon film and allowing it to dry at room temperature. Before imaging, dried specimens were sputter-coated with approximately 5-nm gold film using a Denton sputter-coater. Energy dispersive X-ray spectroscopy was utilized on non-coated specimens dried from aqueous solutions on Si wafers at 15 kV. For pore size distribution, at least 20 particles of each type were analyzed.

**ζ-Potential measurements.** ζ-Potential of hydrogel particles on manganese oxide cores was monitored using Nano Zetasizer (Malvern). For pH-dependent ζ-potential measurements of the particles, their suspensions were centrifuged, supernatants were removed and 0.01 M NaH<sub>2</sub>PO<sub>4</sub> solutions at appropriate pH were added, followed by redispersion on a shaker and sonication for 1 min. In every case, a zeta potential value was obtained by averaging three independent measurements (each of 20 runs).

**Characterization of porous templates.** The surface areas and porosities of manganese oxide particles were analyzed by physisorption using Micromeritics ASAP 2020. Before analysis, the samples were degassed at 30°C and 100°C and nitrogen adsorption was performed at -196°C for relative pressures between 1 and 100%.

**Cell studies.** Two cell lines (HeLa, human cervical carcinoma cells; and HEK293, human embryonic kidney cells) were used for non-loaded hydrogel particles cytotoxicity studies. Cells were seeded in wells of a 96-well tissue culture plate at a density of  $2 \times 10^4$  cells/well in DMEM (high glucose) supplemented with 10% heat-inactivated fetal bovine serum, and incubated with the particles at a particle-to-cell ratio of 100. Incubation was carried out at 37 °C in an atmosphere of humidity  $\geq 85\%$  and air/CO<sub>2</sub> ratio of 95/5%. Subsequently, at 24-h intervals (Days 1, 2, and 3) 100 μL of Cell Titer-Glo reagent (Promega Inc.) was added to each well and the plates were incubated for an additional 10 min at room temperature on an orbital shaker at 300 rpm. At the end of the incubation, luminescence was measured using a multi-label reader (Envision, PerkinElmer, Wellesley, MA) with an integration time of 0.1 s. Each treatment was analyzed in six replicates. Data were used to calculate cell viability relative to untreated controls.

The anticancer potential of DOX-loaded hydrogel particles was studied using A549 (human alveolar adenocarcinoma) and HeLa cancer cells. The cells were plated in clear-bottom 96-well black plates at ~25000 cells/well. After cell counting, hydrogel particles containing doxorubicin hydrochloride (DOX-cubes) were added at 100 particles/cell (six replicates for each condition). Particle-free supernatant of the DOX-cubes suspension was used as a negative control. The same volume of supernatant as that of DOX-cubes suspension was used for each case. DOX solution was used as a positive control of cytotoxicity at 1 μM. The cells exposed to the DOX-cubes, the particle-free supernatant or DOX solution was incubated at 37°C, 5% CO<sub>2</sub> for 24, 48 and 72 hours. After each time point, 100 μl of Cell Titer-Glo reagent was added to each well to

determine cytotoxicity. GraphPad Prism software was used for statistical analysis. A statistical t-test (no parametric) was used to compare the mean values of cells exposed to DOX-cubes and the negative control.

Figures

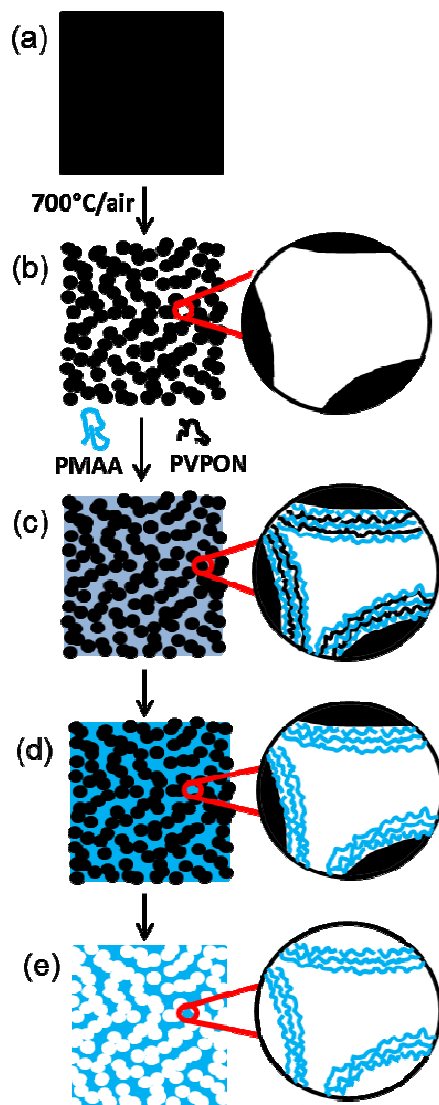


**Figure 1.** Non-porous MnCO<sub>3</sub> cubic particles (a) transformed into porous Mn<sub>2</sub>O<sub>3</sub> cubic particles (b) upon heating at 700°C in air. Hydrogen-bonded PMAA/PVPON complexes formed inside pores of PEI-coated templates (c) were cross-linked with ethylenediamine to form an interconnected PMAA hydrogel network (d). After core dissolution, responsive hydrogel cubes of interconnected PMAA networks are formed (e).

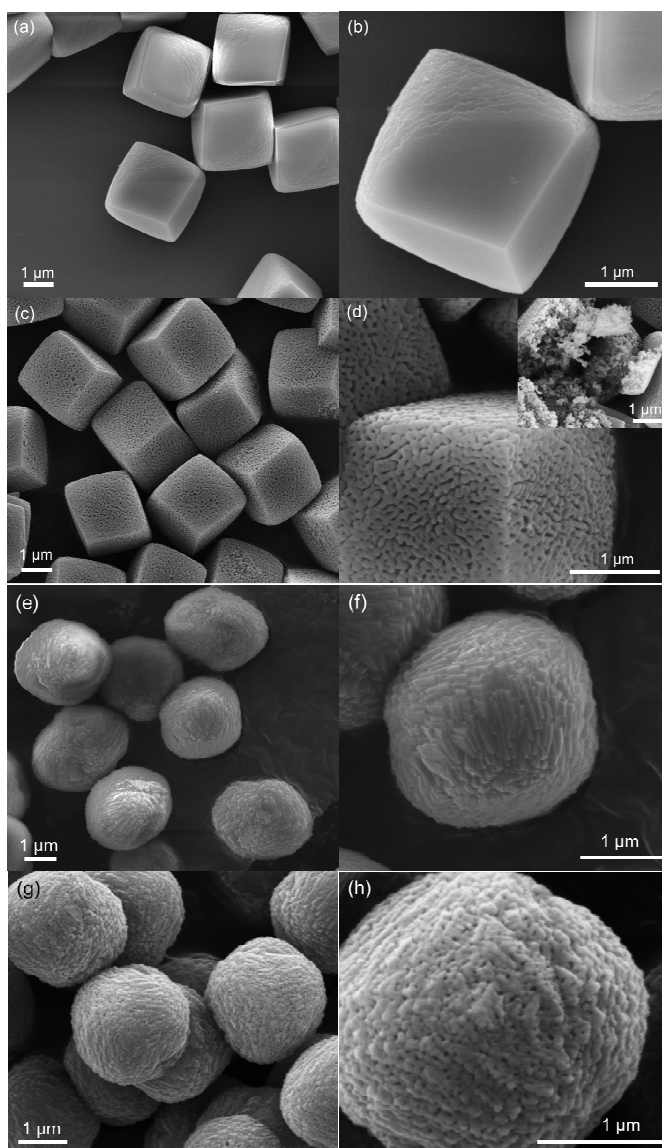


**Figure 2.** SEM images of 2- $\mu\text{m}$   $\text{MnCO}_3$  cubic and spherical particles as-synthesized (a, b, e, f) and after heat-induced transformation to porous manganese (III) oxide cubes and spheres (c, d, g, h). Inset shows the interior of the porous particle.

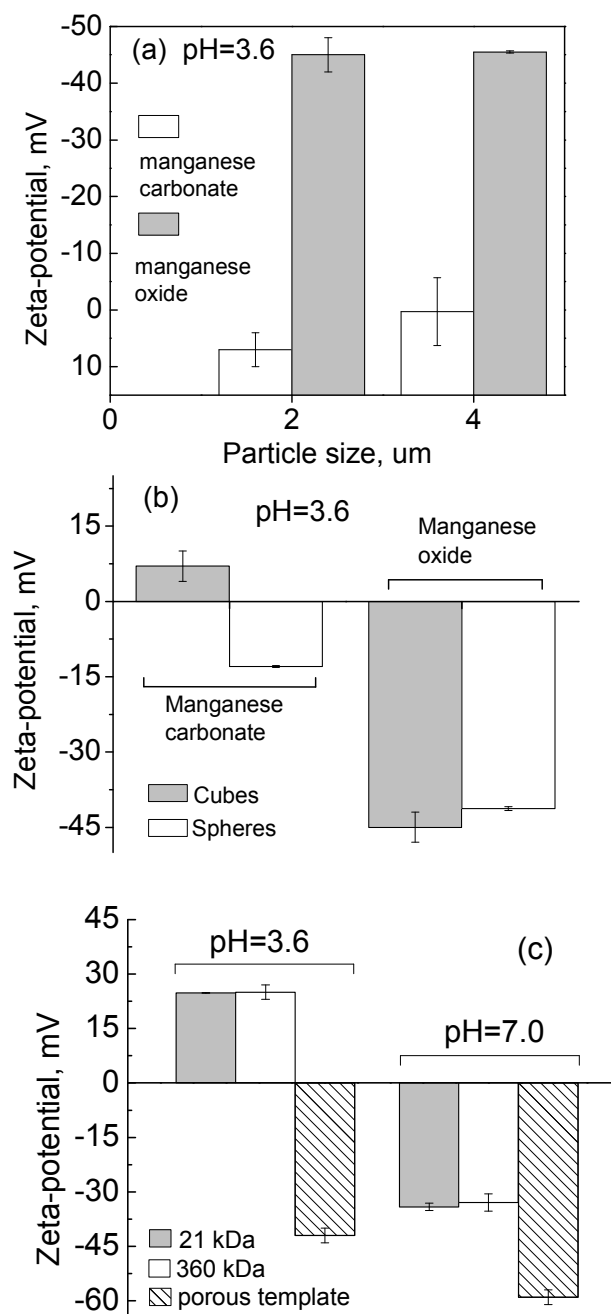


**Figure 3.** (a)  $\zeta$ -Potential measurements of non-porous manganese carbonate and porous manganese oxide cubes of 2  $\mu\text{m}$  and 4  $\mu\text{m}$ , and (b) of 2  $\mu\text{m}$  particles of cubic and spherical shape. Measurements were performed with particles in 0.01 M phosphate solutions at pH=3.6. (c) pH-Dependent  $\zeta$ -potential variations of porous non-modified 2  $\mu\text{m}$  cubes (striped), and those modified with multilayer hydrogel interconnected networks of PMAA with  $M_w$  21 kDa (filled grey) and  $M_w$  360 kDa (clear).

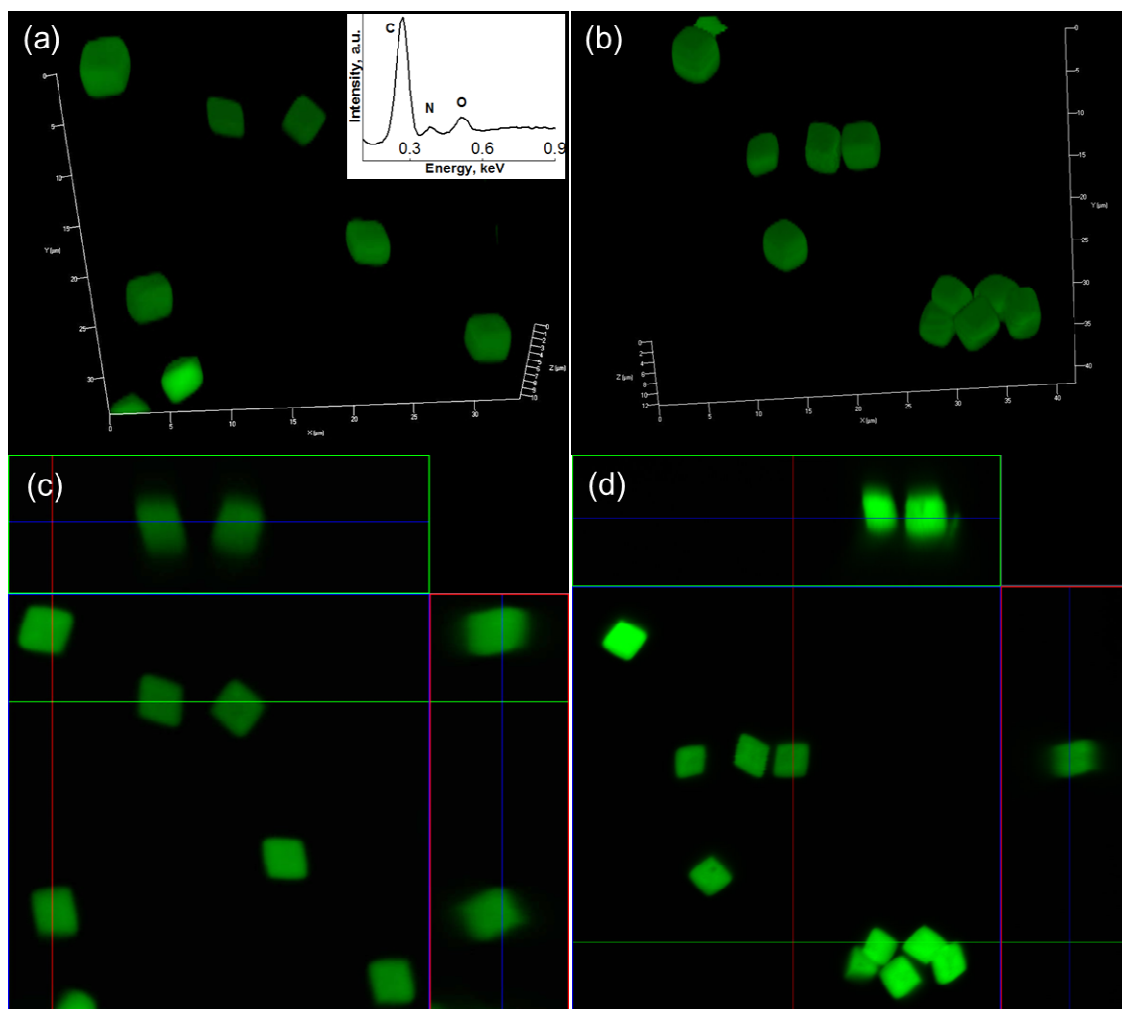


**Figure 4.** Three-dimensional reconstructions of consecutive focal plane confocal microscopy images of 2- $\mu\text{m}$  cubic hydrogel particles made from PMAA of (a) 21 kDa and (b) 360 kDa with their corresponding orthogonal (side panel) views (c) and (d), respectively. The particles were imaged in 0.01 M phosphate buffer solutions at pH=7.4. Inset shows an EDX spectrum of dried hydrogel particles from (a).

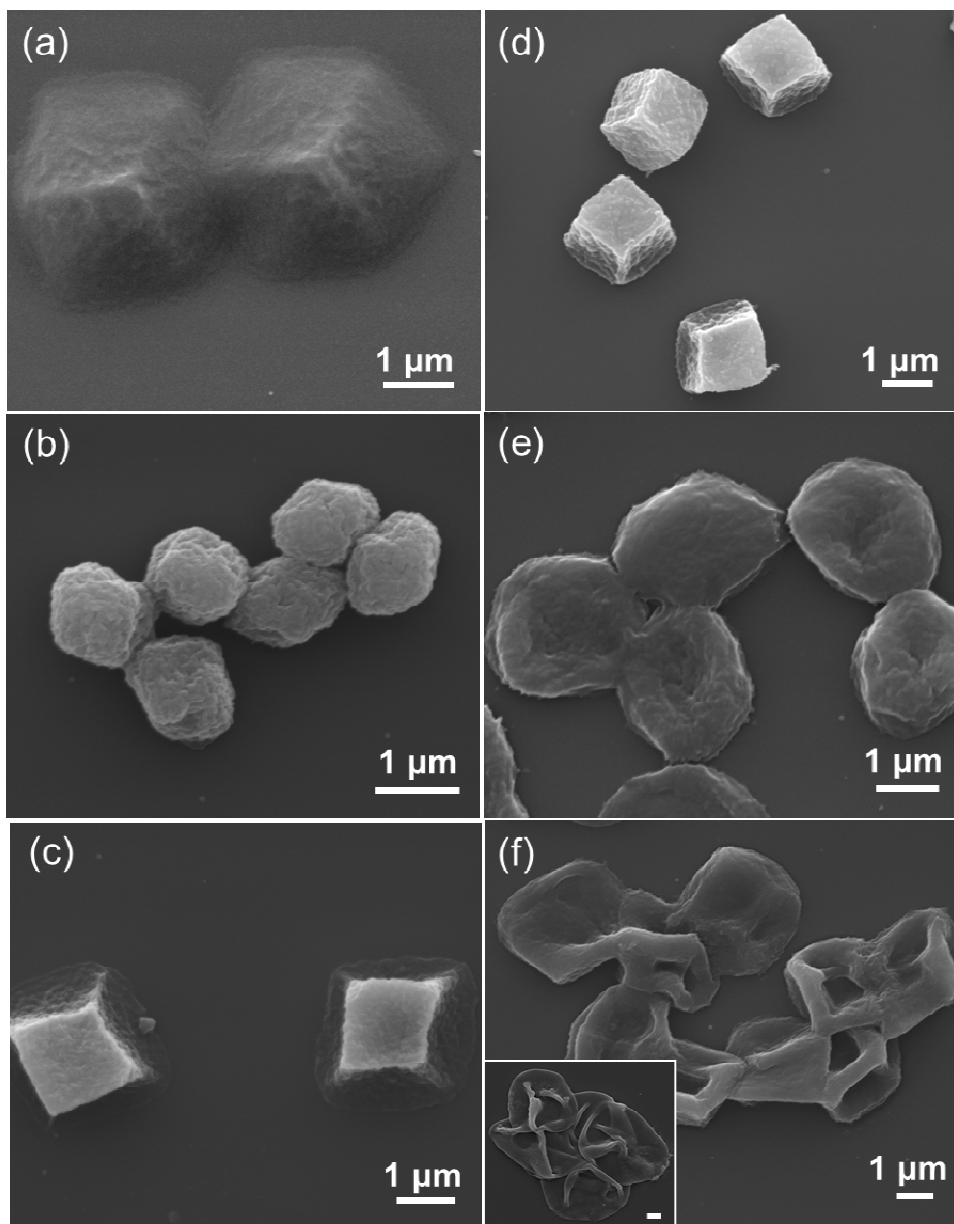


**Figure 5.** SEM images of (PMAA) hydrogel particles obtained from 21 kDa PMAA (a,b,c) and 360 kDa PMAA (d,e,f) using 2- $\mu\text{m}$  cubic (a,d), and spherical (b,e), and 4- $\mu\text{m}$  cubic porous manganese oxide templates. Inset shows 20-layer (PMAA) cubic capsules assembled on nonporous  $\text{MnCO}_3$  templates. The inset scale bar is 1  $\mu\text{m}$ .

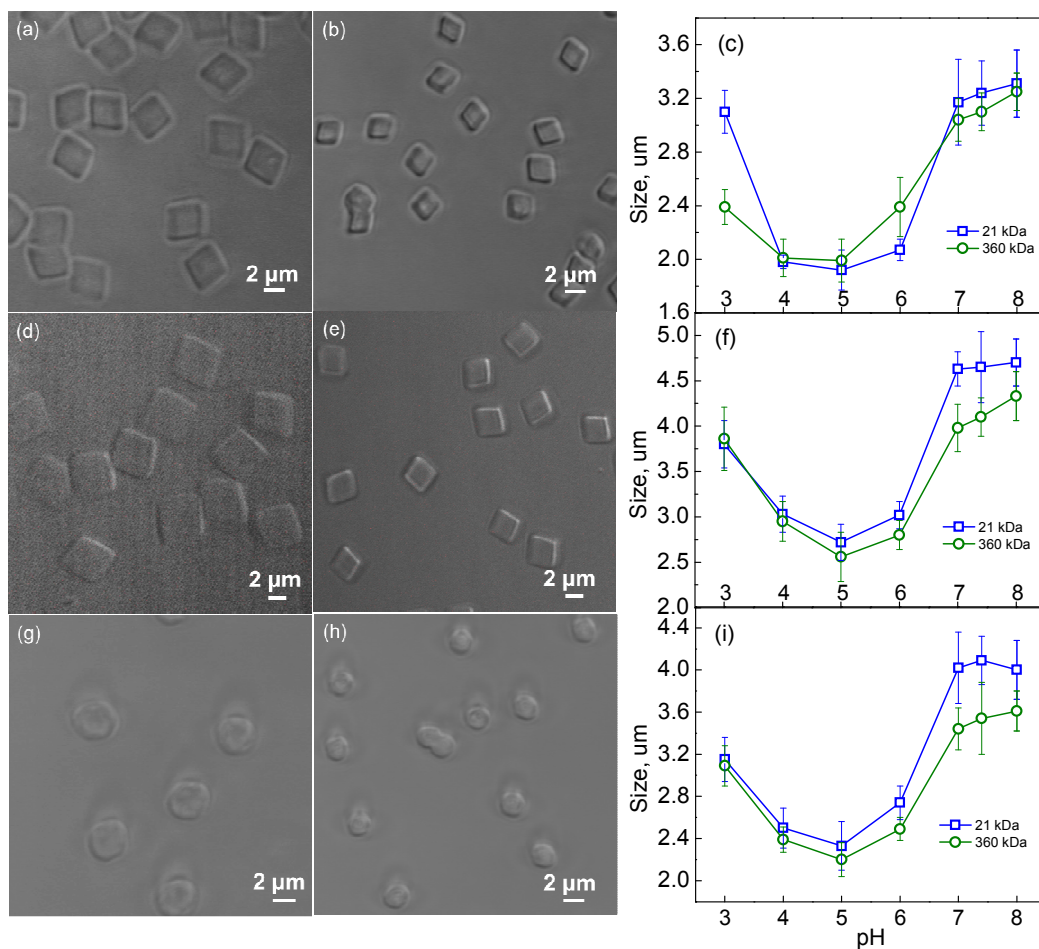


**Figure 6.** Left: Optical microscopy images of 2- $\mu\text{m}$  cubic (21 kDa PMAA) (a, b), 4- $\mu\text{m}$  cubic (21 kDa PMAA) (d, e), and 2- $\mu\text{m}$  spherical (360 kDa PMAA) (g, h) particles imaged at pH=7.4 (a, d, g) and at pH=5 (b, e, h). Right: pH-Induced size variations of 2- $\mu\text{m}$  cubic (c), 4- $\mu\text{m}$  cubic (f), and 2- $\mu\text{m}$  spherical (i) PMAA hydrogel particles produced from 21 kDa or 360 kDa PMAA. The size measurements were performed using confocal microscopy.

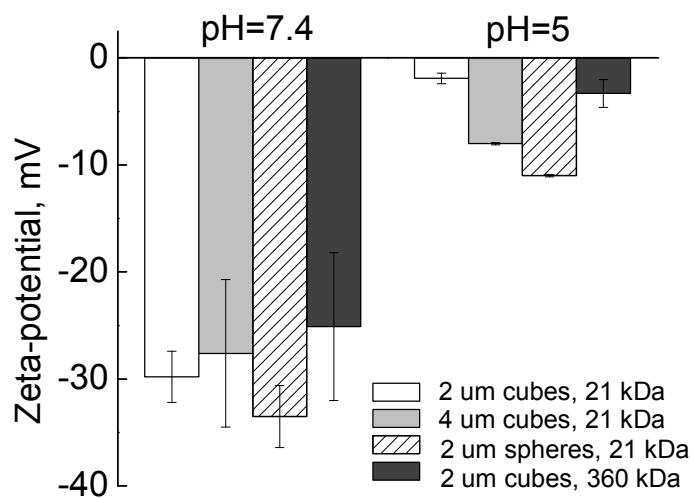


**Figure 7.** pH-Dependent  $\zeta$ -potential variations of PMAA hydrogel particles produced from 21 kDa or 360 kDa PMAA.

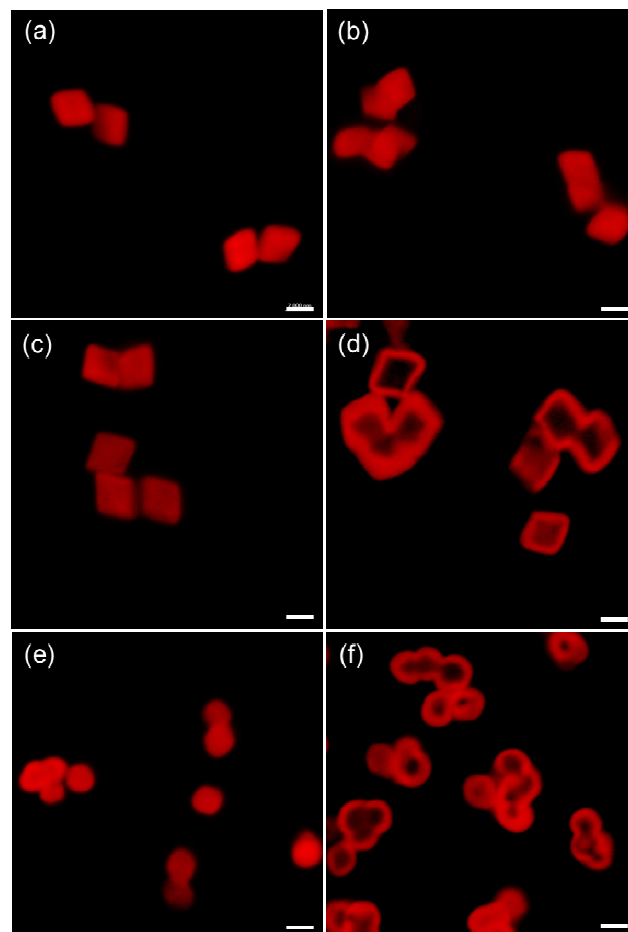


**Figure 8.** CLSM images of DOX-loaded hydrogel cubes of 2- $\mu\text{m}$  (a, b), or of 4- $\mu\text{m}$  (c), 2- $\mu\text{m}$  hydrogel spheres (e). Hollow 4- $\mu\text{m}$  cubic (d) or 2- $\mu\text{m}$  spherical (f) thick-wall PMAA hydrogel capsules. 21 kDa PMAA (a,c,e) or 360 kDa PMAA (b, d, f) were used for the hydrogel assembly. The particles were imaged in solutions at pH=7.4 (0.01 M phosphate). Scale bar is 2  $\mu\text{m}$ .

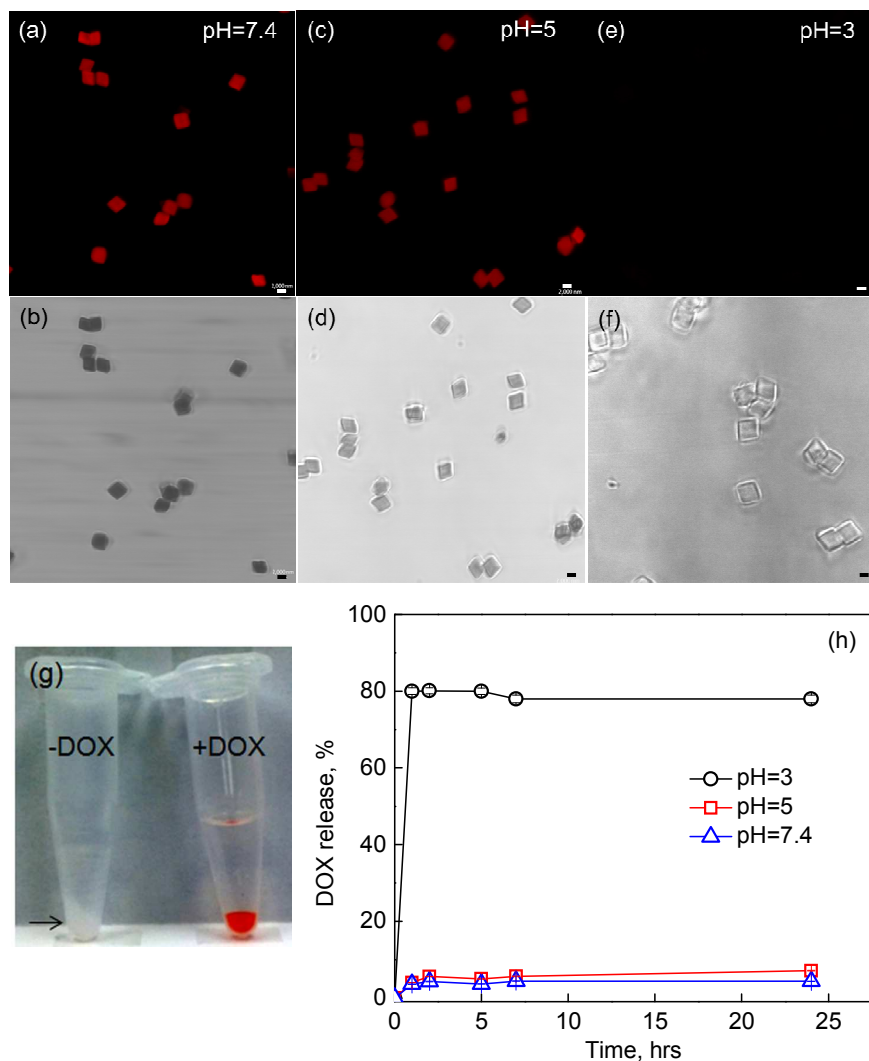


**Figure 9.** Confocal microscopy (top panels) and corresponding transmitted light (bottom panels) images of 4- $\mu\text{m}$  cubic PMAA (21 kDa) hydrogel particles loaded with DOX and consequently exposed to solutions at pH=7.4 (a,b), pH=5 (c,d) and pH=3 (e,f). Scale bar is 2  $\mu\text{m}$ . (g) A photograph of 2  $\mu\text{m}$  cubic gels of (PMAA)<sub>7</sub> (21 kDa) before and after DOX loading. (h) pH-dependent release of DOX from 2- $\mu\text{m}$  cubic gels of (PMAA)<sub>7</sub> (21 kDa). DOX was loaded into the hydrogel cubes by incubation of the particles in 0.2 mg mL<sup>-1</sup> DOX solution (pH=6.4, 0.01 M phosphate) for 24 h. DOX-loaded cubic hydrogels were exposed to 0.01 M phosphate buffers at pH=7.4 (triangles), pH=5 (squares), and pH=3 (circles) for certain periods of time and DOX release was measured using UV-Vis spectroscopy.

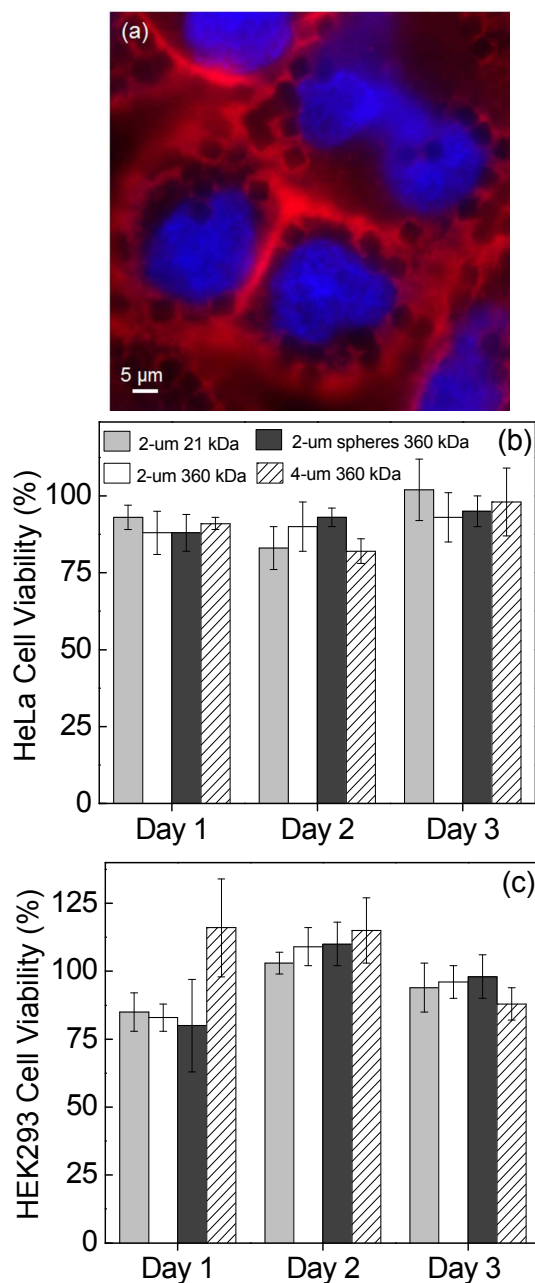


**Figure 10.** (a) A representative optical image of A549 cells with internalized 2 μm cubic hydrogels (21 kDa PMAA) with cell nuclei stained in blue (DAPI) and actin filaments stained in red (AlexaFluor594-conjugated phalloidin). Viability of HeLa and HEK293 cells (%) measured after 24-, 48, and 72-h incubation of cells with 2-μm and 4-μm cubic and 2-μm spherical PMAA particles. Human cancer cells, HeLa (a) or HEK293 (b) were plated in the wells of black 96-well plates at a density of  $2 \times 10^4$  cells/well. After overnight incubation, cells were incubated with 2-

$\mu\text{m}$  cubic (21 kDa PMAA) (light grey), 2- $\mu\text{m}$  cubic (360 kDa PMAA) (white), 2- $\mu\text{m}$  spherical (21 kDa PMAA) (dark grey), and 4- $\mu\text{m}$  cubic (21 kDa PMAA) (striped) particles at cell-to-particle ratio of 1:100. Each data point represents an average of six replicates  $\pm$  std. dev.

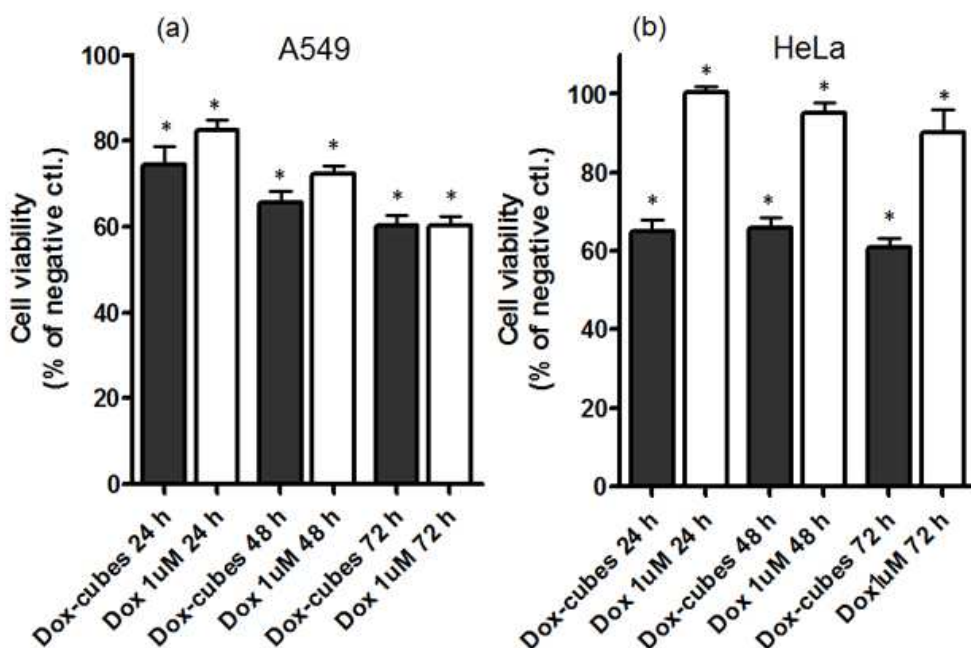


**Figure 11.** Viability of A549 and HeLa cells (% of negative control) measured after 24-, 48, and 72-h incubation of cells with 2- $\mu\text{m}$  DOX-loaded cubic hydrogels of 21 kDa PMAA (DOX-cubes). Human cancer cells, A549 (a) or HeLa (b) were plated at a density of  $2.5 \times 10^4$  cells/well. After overnight incubation, cells were incubated with DOX-cubes at cell-to-particle ratio of 1:100. Particle-free supernatant of the DOX-cubes suspension was used as a negative control with the same volume as that of DOX-cubes suspension. DOX solution (1  $\mu\text{M}$ ) was used as a positive control of cytotoxicity. Each data point represents an average of six replicates  $\pm$  std. dev. Mean values were significantly different ( $*p < 0.05$ , t-test no parametric) from the negative control.

## References

- 1 Y. Osada, J. P. Gong and Y. Tanaka, *J. Macromol. Sci., C: Polymer Reviews*, 2004, **44**, 87.
- 2 T. Tanaka and D. J. Fillmore, *J. Chem. Phys.*, 1979, **70**, 1214.
- 3 (a) D. J. Beebe, J. S. Moore, J. M. Bauer, Q. Yu, R. H. Liu, C. Devadoss and B.-H. Jo, *Nature*, 2000, **404**, 588. (b) B. Zhao and J. S. Moore, *Langmuir*, 2001, **17**, 4758. (c) N. Peppas and W. Leobandung, *J. Biomater. Sci. Polym. Ed.*, 2004, **15**, 125. (d) J. H. Holtz and S. A. Asher, *Nature*, 1997, **389**, 829. (e) Y.-J. Lee, S. A. Pruzinsky and P. V. Braun, *Langmuir*, 2004, **20**, 3096. (f) M. Leonard, M. R. De Boisseson, P. Hubert, F. Dalencion and E. Dellacherie, *J. Controll. Release*, 2004, **98**, 395.
- 4 (a) N. Rapoport, *Progress in Polymer Science*, 2007, **32**, 962. (b) B. H. Tan and K. C. Tam, *Advances in Colloid and Interface Science*, 2008, **136**, 25. (c) E. Costa, M. M. Lloyd, C. Chopko, A. Aguiar-Ricardo and P. T. Hammond, *Langmuir*, 2012, **28**, 10082. (d) A. Wang, Y. Cui, J. Li and J. C. van Hest, *Adv. Func. Mater.*, 2012, **22**, 2673. (e) M. Motornov, Y. Roiter, I. Tokarev and S. Minko, *Progress in Polymer Science*, 2010, **35**, 174. (f) J. F. Mano, *Adv. Eng. Mater.*, 2008, **10**, 515.
- 5 J.-W. Yoo, N. Doshi and S. Mitragotri, *Adv. Drug Deliv. Rev.*, 2011, **63**, 1247.
- 6 J. P. Best, Y. Yan and F. Caruso, *Adv. Healthcare Mater.*, 2012, **1**, 35.
- 7 Y. Liu, J. Tan, A. Thomas, D. Ou-Yang and V. R. Muzykantov, *Ther. Deliv.*, 2012, **3**, 181.
- 8 J. A. Champion, Y. K. Katare and S. Mitragotri, *J. Control. Release*, 2007, **121**, 3.
- 9 P. Decuzzi and M. Ferrari, *Biophys. J.*, 2008, **94**, 3790.
- 10 H. Meng, S. Yang, Z. Li, T. Xia, J. Chen, Z. Ji, H. Zhang, X. Wang, S. Lin, C. Huang, Z. H. Zhou, J. I. Zink and A. E. Nel, *ACS Nano*, 2011, **5**, 4434.
- 11 J. Wang, J. D. Byrne, M. E. Napier and J. M. DeSimone, *Small*, 2011, **7**, 1919.
- 12 J. Champion and S. Mitragotri, *Pharmaceutical Research*, 2009, **26**, 244.
- 13 L. Tao, W. Hu, Y. Liu, G. Huang, B. D. Sumer and J. Gao, *Experimental Biology and Medicine*, 2011, **236**, 20.
- 14 J. Chen, V. Kozlovskaya, A. Goins, J. Campos-Gomez, M. Saeed and E. Kharlampieva, *Biomacromolecules*, 2013, DOI: 10.1021/bm4008666.
- 15 S. Shah, Y. Liu, W. Hu and J. Gao, *Nanosci. Nanotechnol.*, 2011, **11**, 919.
- 16 L. E. Euliss, J. A. DuPont, S. Gratton and J. M. DeSimone, *Chem. Soc. Rev.*, 2006, **35**, 1095.
- 17 Y. Wang, J. D. Byrne, M. E. Napier and J. M. DeSimone, *Adv. Drug Deliv. Rev.*, 2012, **64**, 1021.
- 18 Y. Geng, P. Dalhaimer, S. Cai, R. Tsai, M. Tewari, T. Minko and D. E. Discher, *Nat. Nanotech.*, 2007, **2**, 249.
- 19 S. Muro, C. Garnacho, J. A. Champion, J. Leferovich, C. Gajewski, E. H. Schuchman, S. Mitragotri, and V. R. Muzykantov, *Mol. Ther.*, 2008, **16**, 1450.
- 20 T. Merkel, S. Jones, K. Herlihy, F. Kersey, A. Shields, M. Napier, J. Luft, H. Wu, W. C. Zamboni, A. Z. Wang, J. E. Bear and J. M. DeSimone, *Proc. Nat. Acad. Sci. U. S. A.*, 2011, **108**, 586.
- 21 S. M. Moghimi, A. C. Hunter and J. C. Murray, *Pharmacol. Rev.*, 2001, **53**, 283.
- 22 F. Gentile, C. Chiappini, D. Fine, R. C. Bhavane, M. S. Peluccio, M. M.-C. Cheng, X. Liu, M. Ferrari and P. Decuzzi, *J. Biomech.*, 2008, **41**, 2312.
- 23 S.-Y. Lee, M. Ferrari and P. Decuzzi, *Nanotechnology*, 2009, **20**, 495101.
- 24 B. Kaehr and J. B. Shear, *Proc. Natl. Acad. Sci. U.S.A.*, 2008, **105**, 8850.

- 25 K. J. Lee, J. Yoon, S. Rahmani, S. Hwang, S. Bhaskar, S. Mitragotri and J. Lahann, *Proc. Natl. Acad. Sci. U.S.A.*, 2012, **109**, 16057.
- 26 P. Calvert, *Adv. Mater.*, 2009, **21**, 743.
- 27 (a) S. Y. Chou, P. R. Krauss and P. J. Renstrom, *Science*, 1996, **272**, 85. (b) S. Q. Xu, Z. H. Nie, M. Seo, P. Lewis, E. Kumacheva, H. A. Stone, P. Garstecki, D. B. Weibel, I. Gitlin and G. M. Whitesides, *Angew. Chem., Int. Ed.*, 2005, **44**, 724. (c) M. Geissler and Y. N. Xia, *Adv. Mater.*, 2004, **16**, 1249. (d) D. K. Hwang, J. Oakey, M. Toner, J. A. Arthur, K. S. Anseth, S. Lee, A. Zeiger, K. J. Van Vliet and P. S. Doyle, *J. Am. Chem. Soc.*, 2009, **131**, 4499. (e) J.-W. Yoo and S. Mitragotri, *Proc. Natl. Acad. Sci. U.S.A.*, 2010, **107**, 11205.
- 28 (a) Y. Lvov, G. Decher and H. Möhwald, *Langmuir*, 1993, **9**, 481. (b) N. Elsner, V. Kozlovskaya, S. A. Sukhishvili and A. Fery, *Soft Matter*, 2006, **2**, 966. (c) M. O. Lisunova, I. Drachuk, O. A. Shchepelina, K. D. Anderson and V. V. Tsukruk, *Langmuir*, 2011, **27**, 11157.
- 29 (a) E. Kharlampieva and S. A. Sukhishvili, *J. Macromol. Sci. C: Polymer Reviews*, 2006, **46**, 377. (b) Z. Tang, Y. Wang, P. Podsiadlo and N. A. Kotov, *Adv. Mater.*, 2006, **18**, 3203. (c) P. T. Hammond, *AIChE Journal*, 2011, **57**, 2928.
- 30 V. Kozlovskaya, E. Kharlampieva, I. Erel and S. A. Sukhishvili, *Soft Matter*, 2009, **5**, 4077.
- 31 S. W. Morton, K. P. Herlihy, K. E. Shopsowitz, Z. J. Deng, K. S. Chu, C. J. Bowerman, J. M. DeSimone and P. T. Hammond, *Adv. Mater.*, 2013, **25**, 4707.
- 32 Y. Wang, A. S. Angelatos and F. Caruso, *Chem. Mater.*, 2008, **20**, 848.
- 33 A. G. Skirtach, A. M. Yashchenok and H. Möhwald, *Chem. Commun.*, 2011, **47**, 12736.
- 34 V. Kozlovskaya, E. Kharlampieva, M. L. Mansfield and S. A. Sukhishvili, *Chem. Mater.*, 2006, **18**, 328.
- 35 (a) M. Matsusaki and M. Akashi, *Expert Opin. Drug Deliv.* 2009, **6**, 1207. (b) W. J. Tong and C. Y. Gao, *J. Mater. Chem.*, 2008, **18**, 3799.
- 36 A. Yashchenok, B. Parakhonskiy, S. Donatan, D. Kohler, A. Skirtach and H. Möhwald, *J. Mater. Chem. B*, 2013, **1**, 1223.
- 37 (a) B. Holt, R. Lam, F. C. Meldrum, S. D. Stoyanov and V. N. Paunov, *Soft Matter*, 2007, **3**, 188. (b) O. Shchepelina, V. Kozlovskaya, E. Kharlampieva, W. Mao, A. Alexeev and V. V. Tsukruk, *Macromol. Rapid Commun.*, 2010, **31**, 2041. (c) E. Donath, S. Moya, B. Neu, G. B. Sukhorukov, R. Georgieva, A. Voigt, H. Baumler, H. Kiesewetter and H. Mohwald, *Chem.-Eur. J.*, 2002, **8**, 5481.
- 38 V. Kozlovskaya, J. Baggett, B. Godin, X. Liu and E. Kharlampieva, *ACS Macro Lett.*, 2012, **1**, 384.
- 39 X. Liang, V. Kozlovskaya, Y. Chen, O. Zavgornodnya and E. Kharlampieva, *Chem. Mater.*, 2012, **24**, 3707.
- 40 P. Lavalley, J. -C. Voegel, D. Vautier, B. Senger, P. Shaah and V. Ball. *Adv. Mater.*, 2011, **23**, 1191.
- 41 D. V. Volodkin, A. I. Petrov, M. Prevot and G. B. Sukhorukov, *Langmuir*, 2004, **20**, 3398.
- 42 Y. Wang, A. Yu and F. Caruso, *Angew. Chem., Int. Ed.*, 2005, **117**, 2948.
- 43 Y. Wang and F. Caruso, *Chem. Mater.*, 2006, **18**, 4089.
- 44 G. Schulz-Ekloff, J. Rathousky and A. Zukal, *Int. J. Inorg. Mater.*, 1999, **1**, 97.
- 45 Y. Zhao, J. Zou, W. Shi and L. Tang, *Microporous Mesoporous Mater.*, 2006, **92**, 251.
- 46 K. Yano and Y. Fukushima, *J. Mater. Chem.*, 2003, **13**, 2577.
- 47 Y. Wang, A. Yu and F. Caruso, *Angew. Chem., Int. Ed.*, 2005, **44**, 2888.
- 48 G. B. Sukhorukov, D. V. Volodkin, A. M. Guenther, A. I. Petrov, D. B. Shenoy and H. Möhwald, *J. Mater. Chem.*, 2004, **14**, 2073.
- 49 Y. Yan, Z. W. Lai, R. J. A. Goode, J. Cui, T. Bacic, M. M. J. Kamphuis, E. C. Nice, and F. Caruso, *ACS Nano*, 2013, **7**, 5558.
- 50 M. Behra, S. Schmidt, J. Hartmann, D. V. Volodkin and L. Hartmann, *Macromol. Rapid Commun.*, 2012, **33**, 1049.
- 51 Y. Wang, A. D. Price and F. Caruso. *J. Mater. Chem.*, 2009, **19**, 6451.
- 52 V. Kozlovskaya, W. Higgins, J. Chen and E. Kharlampieva, *Chem. Commun.*, 2011, **47**, 8352.

- 
- 53 V. Kozlovskaya, Y. Wang, W. Higgins, J. Chen, Y. Chen and E. Kharlampieva, *Soft Matter*, 2012, **8**, 9828.
- 54 I. Haq, E. Matijevic and K. Akhtar, *Chem. Mater.*, 1997, **9**, 2659.
- 55 V. Kozlovskaya and S. A. Sukhishvili, *Macromolecules*, 2006, **39**, 6191.
- 56 E. Kharlampieva, I. Erel-Unal and S. A. Sukhishvili, *Langmuir*, 2007, **23**, 175.
- 57 V. Kozlovskaya, A. Shamaev and S.A. Sukhishvili, *Soft Matter*, 2008, **4**, 1499.
- 58 C. Ortiz and G. Hadziioannou, *Macromolecules*, 1999, **32**, 780.
- 59 E. Urinov, M.Y. Kirgizbayeva, A. S. Kosimov and S. S. Rashidova, *Polymer Science U.S.S.R.*, 1989, **31**, 666.
- 60 P. Knappe, R. Bienert, S. Weidner and A. F. Thünemann, *Polymer*, 2010, **51**, 1723.
- 61 Y. Wang, A. S. Angelatos, D. E. Dunstan and F. Caruso, *Macromolecules*, 2007, **40**, 7594.
- 62 V. Kozlovskaya, O. Zavgorodnya, Y. Wang, J. F. Ankner, E. Kharlampieva, *ACS Macro Letters*, 2013, **2**, 226.
- 63 Y. Wang, V. Bansal, A. N. Zelikin and F. Caruso, *Nano Lett.*, 2008, **8**, 1741.
- 64 (a) S. Sivakumar, V. Bansal, C. Cortez, S. F. Chong, A. N. Zelikin and F. Caruso, *Adv. Mater.*, 2009, **21**, 1820. (b) Y. Yan, A. P. R. Johnston, S. J. Dodds, M. M. J. Kamphuis, C. Ferguson, R. G. Parton, E. C. Nice, J. K. Heath and F. Caruso, *ACS Nano*, 2010, **4**, 2928.
- 65 (a) M. Germain, P. Balaguer, J.-C. Nicolas, F. Lopez, J.-P. Esteve, G. B. Sukhorukov, M. Winterhalter, H. Richard-Foy and D. Fournier, *Biosens. Bioelectron.*, 2006, **21**, 1566, (b) Y. Teramura, Y. Kaneda, T. Totani and H. Iwata, *Biomaterials*, 2008, **29**, 1345, (c) C. M. Goodman, C. M. McCusker, T. Yilmatz and V. M. Rotello, *Bioconjugate Chem.*, 2004, **15**, 897.
- 66 D. Y. Lu, M. Huang, C. H. Xu, W. Y. Yang, C. X. Hu, L. P. Lin, L. J. Tong, M. H. Li, W. Lu, X. W. Zhang, and J. Ding, *BMC Pharmacol.*, 2005, **5**, 11.
- 67 M. Beija, J. -D. Marty and M. Destarac, *Chem. Commun.*, 2011, **47**, 2826.